Multifractal dynamics of turbulent flows in swimming bacterial suspensions

Kuo-An Liu and Lin I

Department of Physics and Center for Complex Systems, National Central University, Jhongli, Taiwan 32001, Republic of China

(Received 20 February 2012; revised manuscript received 17 May 2012; published 24 July 2012)

We experimentally investigate the self-propelled two-dimensional turbulent flows of *Escherichia coli* suspensions in thin liquid films at two different cell concentrations. It is found that the flow has fluctuating vortices with a broad range of scales and intensities through the nonlinear interaction of the swimming bacteria. Increasing cell concentration increases the total propelling power and the nonlinear interaction. It causes the generation of vortices with larger scale, lower frequency, and higher intensity. It also widens the histograms of the flow velocity and the velocity increment between two spatially separated points with more stretched non-Gaussian tails. From the scaling analysis of the structure function $S_q(r)$ of the qth moment of the velocity increment between two points with spatial separation r, nonlinear relations between the scaling exponent ζ_q of $S_q(r)$ and q are found for both cell concentrations, which manifests the multifractal dynamics. The multifractality can be enhanced by increasing cell concentration.

DOI: 10.1103/PhysRevE.86.011924 PACS number(s): 87.18.Gh, 47.53.+n, 47.63.−b, 05.65.+b

I. INTRODUCTION

Turbulence is a state of physical systems with many excited degrees of freedom strongly deviating from equilibrium [1]. It widely exists in different nonlinear extended systems. In hydrodynamic or wave turbulence, the spatiotemporal fluctuation of motion over a broad range of scales is usually associated with power law scaling of the power spectrum [2–4]. Multiscaling and multifractal behaviors have also been observed. Channel flow turbulence [5], gravity–capillary-wave turbulence of surface wave [6], and drift-wave turbulence in tokamak [7,8] are a few good examples. Nevertheless, the above studies have been limited to passive systems under strong external drive and weak dissipation over a broad range of spectra.

Systems such as bacteria [9–25], school of fishes [26], cells [27], and self-propelled particles [28] and rods [29,30] are nonlinearly coupled self-propelled systems exhibiting rich dynamical behaviors. For example, in bacterial suspensions, abnormal diffusion [9–11], enhanced mixing [12], and viscosity reduction [13,14] have been observed. At high cell concentration, hydrodynamic interactions and chemical signal cause strong mutual coupling to correlate bacterial motions [15,31]. The interplay of the above strong mutual coupling, the bacterial self-propelling, and the anisotropic rodlike bacterial shape leads to the self-organized bacterial clustering, coherent motions, or even turbulent flows with fluctuating vortices [16–22].

In hydrodynamic turbulence, energy is usually pumped in from the external drive on a large scale. Through the self-similar cascading of vortices from large scale to small scale, energy is cascaded through the inertial regime in which the Reynolds number Re is large. It leads to the Kolmogorov power law distribution of fluctuations over the broad inertial regime until termination by the strong dissipation at the small scale limit. In contrast, in the dense bacterial flow, Re is much smaller than 1 due to the low speed (a few tens of μm/s) and the small spatial scale (10^{-3}–10^{-1} mm). Intuitively, turbulence cannot occur in the absence of the inertial regime due to the high dissipation. However, the energies that have cascaded from the self-propelled individual bacteria compensate for the dissipation. Cisneros *et al*. proposed an *alternative Reynolds number* Bs, defined as the ratio of thrust forces by dense bacteria to collective dissipation in the collective phase [18]. At high bacterial concentration, Bs $\gg 1$ and bacteria exhibit coherent motion in the form of moving clusters with different scales. The strong nonlinear interaction with neighboring clusters causes growths, disruptions, and velocity variations of clusters. It thereby causes the strong spatial and temporal fluctuations of the velocity field over a broad range of scales. The energies provided by the individual bacteria can thereby cascade to the large scale through the above process, which leads to a flow with the power spectrum following power law scaling over a broad regime. This flow can also be called turbulence because of its excited many degrees of freedom with energy cascading and strong deviation from equilibrium, similarly to other passive turbulence [1].

In previous studies of bacterial turbulence, the distribution and fluctuation of bacterial cluster size and the spatial and the temporal correlations of flow velocity have been used as major measures [16–22]. Whether multiscaling behavior exists and if so what kinds occur are still interesting open questions. In this work, these issues are addressed using *Escherichia coli* (*E. coli*) suspensions in a thin liquid film.

The structure function [7,32,33] is a powerful tool used to investigate the multiscaling dynamics in turbulence. The q-order structure function is defined as $S_q(r) = \langle |v_r|^q \rangle$ for the longitudinal velocity difference $v_r = V_x(x + r, y) - V_x(x, y)$ between two points separated by a distance r, where V_x is the velocity component in the x direction and $\langle \cdots \rangle$ is the ensemble average. For the higher moment q, the large difference in the tail of the histogram of v_r provides a larger contribution to S_q. If the velocity field is self-similar over some range of r, the structure function can be scaled as $S_q(r) \sim r^{\zeta_q}$. In a pure self-similar case without multifractal behaviors, ζ_q is a linear function of q and the system is monofractal. The deviation from the linear relation signifies the multifractal dynamics.

In this work, the scaling behavior of the two-dimensional turbulent bacterial flow with various vortex sizes in a thin liquid film is studied experimentally at two different cell concentrations. The local velocity is obtained through particle

imaging velocimetry (PIV). Conventional measurements of the power spectrum, the spatial and the temporal correlations of velocity, and the histogram of V_x are conducted [18,19]. In addition, the multiscaling behaviors in turbulent bacterial flow are investigated using the histograms of v_r and the structure functions $S_q(r)$. It is found that increasing cell concentration enhances the large-scale vortices with stronger intensities and longer persistent times, broadens the histograms of V_x and v_r, and causes the more stretched non-Gaussian tails. It also leads to the more nonlinear relation between ζ_q and q, which manifests the higher degree of multifractality of the flow dynamics at higher cell concentration.

II. EXPERIMENT

The *E. coli* cells (wild-type RP437) are grown at 37 °C and shaken at 260 rpm in *L* broth (1 wt. % tryptone, 0.5 wt. % yeast extract, and 0.5 wt. % NaCl). Overnight cultures are diluted 1% in *T* broth (1 wt. % tryptone and 0.5 wt. % NaCl), grown at 30 °C, and shaken at 260 rpm. After 4 h, cells are harvested in midexponential phase. The cell concentration of the liquid suspension is measured by optical density (optical absorption) at a wavelength of 600 nm (OD_{600}). In the linear range ($0.1 < A_{OD_{600}} < 0.5$), $A_{OD_{600}} = 0.1$ represents 1×10^8 cells/ml [34]. The cells are then separated from the media by centrifugation (5000 rpm, 10 min), washed, and finally suspended with motility buffer (6.2 mM K_2HPO_4, 3.8 mM KH_2PO_4, 67 mM NaCl, and 0.1 mM ethylenediamine tetra-acetic acid, *p*H 7.0) containing 0.5 wt. % glucose and 0.002 wt. % Tween 20 [23–25]. Then the cells are condensed to two different concentrations of $n \simeq 3 \times 10^{10}$ and 7.5×10^9 cells/ml for runs I and II, respectively.

To prepare the thin liquid film with bacterial suspensions, a homemade system similar to that of Ref. [15] is used. A 0.6-μl drop of bacterial suspension is placed between four movable supporting nylon fibers with a diameter of 20 μm in a chamber with water-saturated air. The drop is stretched to a (3×3)-mm^2 thin film by slowly moving the fibers. The elasticity and surface tension created by the surfactant Tween 20 are sufficient to sustain the film for few minutes. The cell concentration is uniform under the uniform supplies of the primary chemoattractant (oxygen) from both sides of the air-film interfaces and the fast stirring of the fluid by bacteria [15]. Phase contrast images are recorded by a video camera with 640×480 pixels at a 200-Hz sampling rate. The velocity field is extracted from consecutive images by the PIV software MatPIV in MATLAB [35].

III. RESULTS AND DISCUSSION

Figure 1(a) shows typical snapshots of the velocity field represented by arrows at different times for run I (top row) and run II (bottom row). Vortices with different shapes, sizes, and lifetimes coexist. Their corresponding vorticities with two different directions and different strengths are depicted by the colors of the contour plots. The higher cell concentration of run I leads to the appearance of larger and stronger vortices with higher vorticity than those of run II at lower cell concentration. The vortex circled by the large dashed ellipse is a typical example of the large vortex about 110 μm

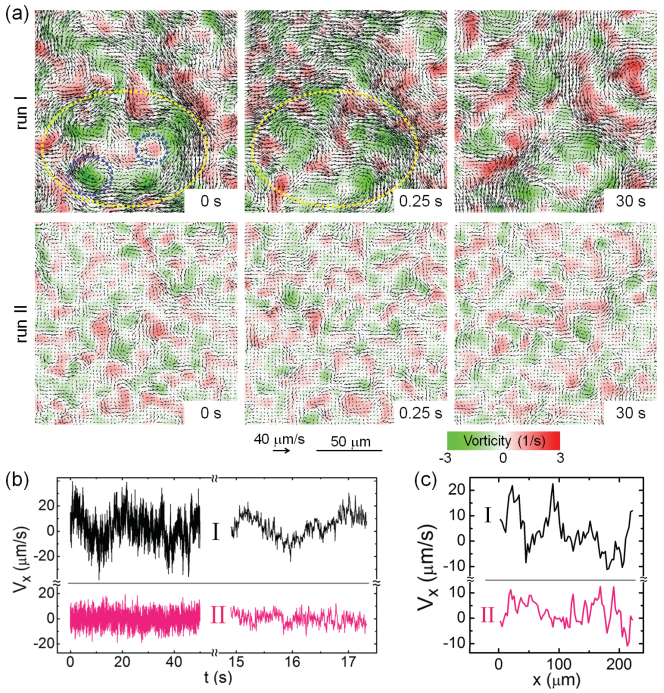

FIG. 1. (Color online) (a) Typical snapshots of the fields of velocity and vorticity at different times for high-cell-concentration run I (top row) and low-cell-concentration run II (bottom row). The arrows correspond to the local velocity and the color reflects the local vorticity. The circled region shows the example of the coexistence of the small vortices inside the large vortex. The large vortex has the longer lifetime. (b) Temporal evolutions of V_x at fixed points for both runs. (c) Spatial evolution of V_x at a fixed time for both runs. The higher-concentration run I exhibits the more turbulent flow with vortices that have larger spatiotemporal scales and larger amplitude fluctuations.

in diameter. Inside the large vortex, the coexisting smaller vortices (circled by the small dashed ellipses) can also be observed. The similar patterns between the left and the middle panels with 0.25-s separation of run I in Fig. 1(a) manifest that the large vortices have lifetimes longer than those of the small vortices. For example, in the large ellipse, the large vortex remains similar, but the small vortices are different. Figure 1(b) depicts the temporal variation of the local velocity V_x in the x direction at a certain fixed point for $t = 0$–50 s. The right column shows the magnified plots. Figure 1(c) shows typical plots of V_x versus x. The stronger fluctuation associated with the increasing intensity of the slower and larger-scale modes of run I is mainly contributed by the larger-scale vortices with slower dynamics. Namely, increasing cell concentration increases the mean lifetime, the mean size, and the mean intensity of vortices. The increase of the standard deviation of the velocity fluctuation from 4.8 to 11 μm/s from run II to run I is further evidence that the flow becomes more turbulent with increasing cell concentration.

The concentration dependence of coherent motions can also be evidenced by the larger width of the longitudinal spatial correlation function C_r [Fig. 2(a)] and the temporal correlation function C_τ [Fig. 2(b)] for V_x from two points at the same y but separated by distance r and time interval τ, with increasing cell concentration. The negative value of

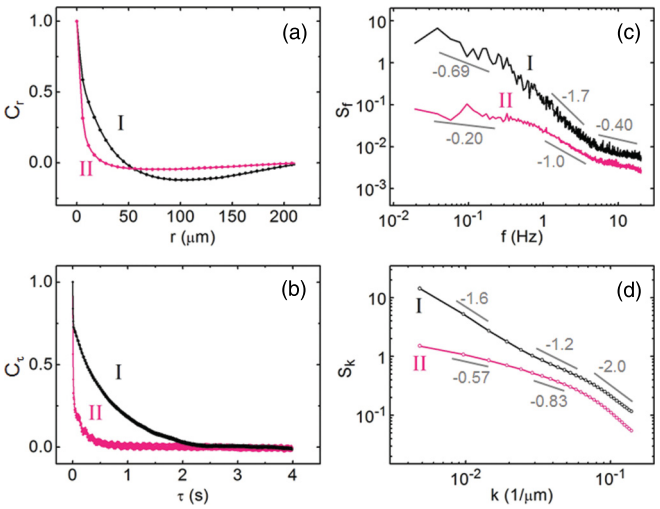

FIG. 2. (Color online) (a) and (b) Plots of the spatial correlation function C_r and the temporal correlation function C_τ of V_x versus r and τ, respectively, for both runs. (c) and (d) Plots of the power spectra of V_x, i.e., S_f and S_k versus f and k, respectively, for both runs. The numbers indicate the scaling exponents of the adjacent gray straight lines.

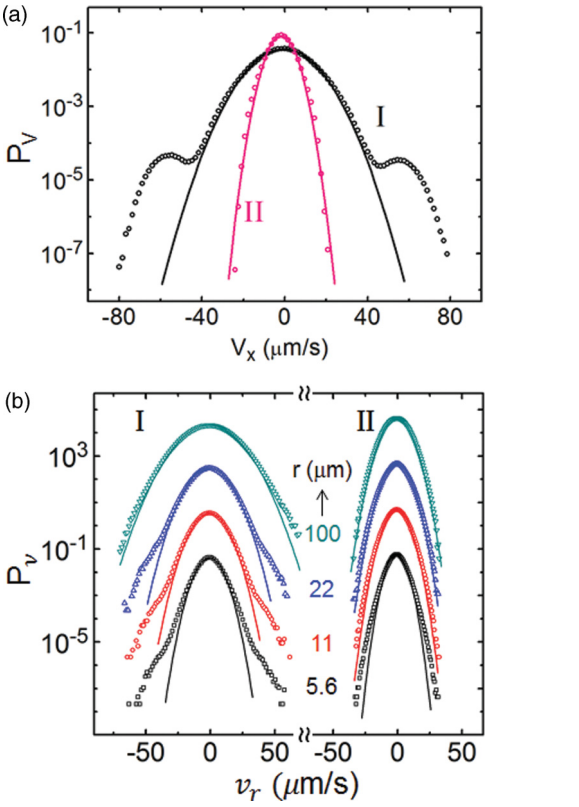

FIG. 3. (Color online) (a) Plots of P_V versus V_x. (b) Plots of P_v versus v_r at different separation r. Solid curves are the best Gaussian fits. Increasing cell concentration from run II to run I not only widens the core of P_V but also induces two humps at the large-$|V_x|$ ends, centered at $V_x = \pm 54.4$ μm/s, which are the typical collective swimming speeds at high cell concentration. The P_v of run I also shows the broader distribution with a more stretched non-Gaussian tail.

C_r results from the two nearest vortices, which tend toward opposite rotating directions. Thus $r = 101$ μm (70 μm) for the most negative value of C_r in run I (II) stands for the mean inter vortex distance of the neighboring large-scale vortices. Here C_τ exhibits two-step relaxation. The decay of C_τ from 1 to 0.85 (0.56) for run I (II) within 5 ms is the fast relaxation. The slow relaxation results from the rearrangement of the coherent motions. The two-step relaxation was also observed in a previous experimental study of bacterial flow on a dense agar gel substrate [19]. However, our fast relaxation time scale is much shorter because the dynamics and the average swimming speeds (~20 and ~10 μm/s for runs I and II, respectively) in our free standing film are 10 times faster than those on their dense agar gel substrate.

Figures 2(c) and 2(d) show the power spectra S_f and S_k, where f and k are the frequency and the wave number, respectively. Over the entire range of both spectra, the higher-concentration run I has larger intensities than the lower-concentration run II. The nearly parallel curves for the two runs in each spectrum at the high-f and the high-k ends could be mainly attributed to the individual high-frequency and short-range motion, which is weakly coupled. The increasing deviations of the two curves toward the low-f and the low-k ends manifest the easier generation of the slow and large-scale vortices under the effects of increasing nonlinear interaction and energy input with increasing concentration [15,17,22,25].

Note that unlike hydrodynamic turbulence, bacterial flow is highly dissipative. The local energy injected by the self-propelled bacteria provides a source to sustain the inverse energy cascade under strong dissipation. A bacterial swimming number $\mathrm{Bs} = F_n/F_\mu = 6\pi naL^2 v/U$ proposed by Cisneros *et al.* [18] is an alternative Reynolds number used to explain the possibility of turbulent flow when $\mathrm{Re} \ll 1$. Here F_n and F_μ are the force density provided by the bacteria and the viscous dissipation force density in the collective phase, respectively; L, a, n, v, and U are the observed correlation length, cell radius, cell concentration, speed of the single-cell motion, and speed of the collective motion, respectively. In our experiments, n is about 10^{10}–10^{11} cells/ml, $a \sim 0.5$ μm, $L \sim 100$ μm, and $v/U \sim 1$. In addition, Bs is about 10^3–10^4, which explains the presence of turbulence without an inertial regime.

Figure 3(a) shows P_V, the probability distribution function (PDF) of V_x. The solid smooth curves are the best Gaussian fits. The P_V of run II shows the nearly Gaussian distribution. Increasing cell concentration not only widens the core of the P_V but also induces two humps at the large-$|V_x|$ ends, centered at $V_x = \pm 54.4$ μm/s. The emergence of the hump at the large-$|V_x|$ end at high cell concentration was also reported by Peruani [36]. It could be attributed to the stronger large-scale cooperative motion with increasing nonlinear interaction and the larger total input of driving energy.

Beyond the above conventional measurements, let us explore the multiscaling behavior of the dynamics. In previous studies of hydrodynamic turbulence, the multifractal scaling behaviors of the dynamics were examined by computing the q-order structure functions $S_q(r) = \langle |v_r|^q \rangle$ of the longitudinal

velocity increment [7,32,33], namely,

$$S_q(r) = \int P_v |v_r|^q dv_r, \tag{1}$$

where P_v is the PDF of the longitudinal velocity increment $v_r = V_x(x+r,y) - V_x(x,y)$ between two points separated by a distance r at fixed y.

Figure 3(b) depicts P_v at different r. The solid smooth curves correspond to the best Gaussian fits. The P_v of run II shows the nearly Gaussian distribution. Increasing cell concentration broadens the distribution. For example, from run II to run I, the standard deviations of v_r at $r = 5.6$ and 100 μm increase by factors of 1.3 and 2.0, respectively. It again manifests the more turbulent flow at the higher cell concentration. The P_v of run I also has the more stretched non-Gaussian tail under the more coherent large-scale motion. The small-v_r regime is mainly contributed by the small velocity fluctuation belonging to the same vortex or the different vortices with small relative velocity in the x direction. The stretched non-Gaussian tail is mainly contributed by the two points belonging to the different vortices with large velocity deviation. It corresponds to the large abrupt fluctuation in run I of Fig. 1(c). For large r (e.g., 100 μm), the random-phase velocity fluctuations accumulated over the smaller vortices with various sizes suppress the non-Gaussian tail and broaden the distribution core.

The left panels of Figs. 4(a) and 4(b) show plots of S_q versus r. For run I, S_q obeys the power law scaling

$$S_q(r) \sim r^{\zeta_q} \tag{2}$$

with nearly constant ζ_q over a wide range of r. For run II, ζ_q decreases with increasing r. The former indicates that the self-similar power law scaling with a similar dynamical selection rule can be extended to a wide range of r through stronger driving and nonlinear coupling at higher cell concentration. It agrees with the power spectrum with a larger scaling exponent in Fig. 2(d). However, the behavior of run II indicates the much weaker increase of intensity of the vortices with increasing size, reflected by the small scaling exponent in the small-k regime at low cell concentration in Fig. 2(d).

Note that S_q at $q = 2$ corresponds to the variance of v_r. Its scaling exponent $\zeta_2 < 1$ indicates that the change of v_r with r is an antipersistent process due to the presence of many small vortices with similar intensities, similarly to that of the non-Markov subdiffusion process [37]. With increasing cell concentration from run II to run I, ζ_2 becomes larger in the presence of the more turbulent flow with larger fluctuations.

The Lipschitz-Hölder exponent α is defined as the local scaling of the measurement v_r through $|v_r| \sim r^{\alpha}$ [37]. If $P_v \sim r^{-f(\alpha)}$, $S_q(r)$ follows

$$S_q(r) = \int r^{-f(\alpha)+q\alpha} d\alpha \sim r^{\zeta_q}. \tag{3}$$

In addition, P_v decreases and $|v_r|^q$ increases with increasing $|v_r|$. For each q, S_q is dominated by the integrand $r^{-f(\alpha_q)+q\alpha_q}$, which is the maximum value at the optimum $|v_r^*| \sim r^{\alpha_q}$. Therefore, from Eq. (3), ζ_q follows

$$\zeta_q = -f(\alpha_q) + q\alpha_q, \tag{4}$$

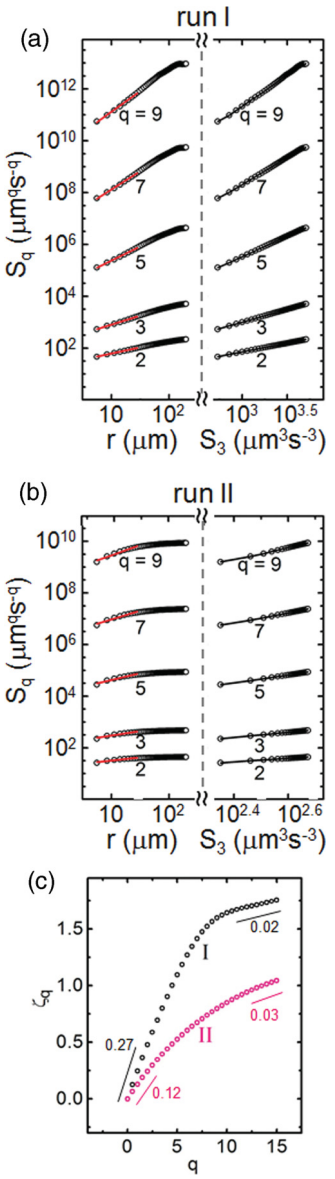

FIG. 4. (Color online) (a) and (b) Plots of S_q versus r and S_3 at different q, respectively. The red straight lines are the best fits for the power law scaling $S_q(r) \sim r^{\zeta_q}$. The constant scaling exponent over a wider region for run I shows that the similar dynamical selection rule can be extended to a wider range of r at higher cell concentration. The constant scaling exponent of the power law scaling between S_q and S_3 for both runs over the whole range of S_3 indicates that ESS holds. (c) Plot of ζ_q versus q. The slopes of the adjacent straight lines indicated by the numbers correspond to the Lipschitz-Hölder exponent α_q. The nonlinear relation between ζ_q and q is evidence of the multifractal nature of the dynamics.

where α_q can be determined from the following equation:

$$\frac{d}{d\alpha}\{-f(\alpha) + q\alpha\}\Big|_{\alpha=\alpha_q} = 0. \tag{5}$$

From Eqs. (4) and (5),

$$\alpha_q = \frac{d}{dq}\zeta_q \tag{6}$$

can be obtained.

The S_q is dominated by the small (large) $|v_r^*|$ for the small (large) q. The scaling behavior of S_q at larger q corresponds to testing the scaling behavior in r space for large $|v_r|$ events. The scaling exponents ζ_q versus q are plotted in Fig. 4(c). The slopes at different q represent the scaling exponent α_q for the corresponding dominated $|v_r|$. For run I, ζ_q is linear with q in the low-q regime with $\alpha_q = 0.27$. However, for $q > 5$, the ζ_q curve starts to bend and α_q reaches 0.02. The nonconstant slope of the nonlinear ζ_q-q curve implies multiple values of α_q and thereby the multifractal dynamics of the turbulence. It can be attributed to the non-Gaussian tail of P_v, which plays a more important role at large q. In contrast to run I, the scaling exponents for run II show weaker nonlinearity with $\alpha_q = 0.12$ and 0.03 at the low- and high-q ends, respectively. This implies that the more turbulent flow with increasing cell concentration exhibits a higher degree of multifractality. Note that for the same q, the wider spread distribution of run I makes $|v_r^*|$ larger than that of run II. Namely, at the high-q end, the more serious bending of ζ_q probes α_q of the larger $|v_r^*|$ from the more stretched non-Gaussian tail of the P_v curves of run I in Fig. 3(b). Also note that for the hydrodynamic turbulent flow, $\alpha_q = 1/3$ (i.e., $\zeta_q = q/3$) in the small-q regime [2]. The reason for the deviation between our results and those of the hydrodynamic turbulent flow needs to be further investigated theoretically.

Finally, from the scaling relation between S_q and S_3 [right panels of Figs. 4(a) and 4(b)], we examine the extended self-similarity (ESS) that holds in hydrodynamic turbulence [38]. The constant scaling exponent over a wide range of S_3 is evidence that ESS also exists in the self-propelled dissipative bacterial flow.

IV. CONCLUSION

In conclusion, we experimentally investigated the self-propelled two-dimensional turbulent flows of *Escherichia coli* suspensions in thin liquid films at two different cell concentrations and observed evidence of multiscaling behavior. The interplay of self-propulsion, the nonlinear interaction, and the rodlike geometry of the swimming bacteria lead to the formation of turbulent flow consisting of vortices of various sizes and intensities. Increasing cell concentration enhances the total self-propelling power and the mutual interaction, which generate larger and stronger vortices with longer persistent time and lower frequency. It broadens the histograms of V_x and v_r and causes the formation of the stretched non-Gaussian tails. The nonlinear relation between q and the scaling exponent ζ_q of the structure function S_q manifests the multifractal scaling of the turbulent flow, which can be enhanced by increasing cell concentration. Comparing to passive hydrodynamic turbulence and wave turbulence, which have energy cascading in the opposite direction in k space and low dissipation in the broad inertia range, a similar finding of multifractal dynamics in our system could shed some light on the study and the understanding of the generic multiscaling behaviors in other coupled self-propelled dissipative systems.

ACKNOWLEDGMENTS

The authors would like to thank Professor Chien-Jung Lo for providing the *E. coli* cells. This work was supported by the National Science Council of the Republic of China under Contract No. NSC99-2112-M-008-002-MY3.

[1] G. Falkovich, K. Gawedzki, and M. Vergassola, Rev. Mod. Phys. **73**, 913 (2001).
[2] U. Frisch, *Turbulence: The Legacy of A. N. Kolmogorov* (Cambridge University Press, Cambridge, 1995).
[3] M. Yamada and K. Ohkitani, Phys. Rev. Lett. **60**, 983 (1988).
[4] X. Z. Wu, L. Kadanoff, A. Libchaber, and M. Sano, Phys. Rev. Lett. **64**, 2140 (1990).
[5] F. Toschi, G. Amati, S. Succi, R. Benzi, and R. Piva, Phys. Rev. Lett. **82**, 5044 (1999).
[6] E. Falcon, S. Fauve, and C. Laroche, Phys. Rev. Lett. **98**, 154501 (2007).
[7] S. Futatani, S. Benkadda, Y. Nakamura, and K. Kondo, Phys. Rev. Lett. **100**, 025005 (2008).
[8] N. Kukharkin, S. A. Orszag, and V. Yakhot, Phys. Rev. Lett. **75**, 2486 (1995).
[9] X. L. Wu and A. Libchaber, Phys. Rev. Lett. **84**, 3017 (2000).
[10] K. C. Leptos, J. S. Guasto, J. P. Gollub, A. I. Pesci, and R. E. Goldstein, Phys. Rev. Lett. **103**, 198103 (2009).
[11] G. Miño, T. E. Mallouk, T. Darnige, M. Hoyos, J. Dauchet, J. Dunstan, R. Soto, Y. Wang, A. Rousselet, and E. Clement, Phys. Rev. Lett. **106**, 048102 (2011).
[12] A. Sokolov, R. E. Goldstein, F. I. Feldchtein, and I. S. Aranson, Phys. Rev. E **80**, 031903 (2009).
[13] A. Sokolov and I. S. Aranson, Phys. Rev. Lett. **103**, 148101 (2009).
[14] B. M. Haines, A. Sokolov, I. S. Aranson, L. Berlyand, and D. A. Karpeev, Phys. Rev. E **80**, 041922 (2009).
[15] A. Sokolov, I. S. Aranson, J. O. Kessler, and R. E. Goldstein, Phys. Rev. Lett. **98**, 158102 (2007).
[16] C. Dombrowski, L. Cisneros, S. Chatkaew, R. E. Goldstein, and J. O. Kessler, Phys. Rev. Lett. **93**, 098103 (2004).
[17] I. S. Aranson, A. Sokolov, J. O. Kessler, and R. E. Goldstein, Phys. Rev. E **75**, 040901(R) (2007).
[18] L. H. Cisneros, R. Cortez, C. Dombrowski, R. E. Goldstein, and J. O. Kessler, Exp. Fluids **43**, 737 (2007).
[19] H. P. Zhang, A. Beer, R. S. Smith, E. L. Florin, and H. L. Swinney, Europhys. Lett. **87**, 48011 (2009).
[20] S. M. Fielding, D. Marenduzzo, and M. E. Cates, Phys. Rev. E **83**, 041910 (2011).
[21] K. Drescher, J. Dunkel, L. H. Cisneros, S. Ganguly, and R. E. Goldstein, Proc. Natl. Acad. Sci. USA **108**, 10940 (2011).
[22] H. P. Zhang, A. Beer, E. L. Florin, and H. L. Swinney, Proc. Natl. Acad. Sci. USA **107**, 13626 (2010).
[23] D. Giacche, T. Ishikawa, and T. Yamaguchi, Phys. Rev. E **82**, 056309 (2010).
[24] L. G. Wilson, V. A. Martinez, J. Schwarz-Linek, J. Tailleur, P. N. Pusey, W. C. K. Poon, and G. Bryant, Phys. Rev. Lett. **106**, 018101 (2011).
[25] T. Ishikawa, N. Yoshida, H. Ueno, M. Wiedeman, Y. Imai, and T. Yamaguchi, Phys. Rev. Lett. **107**, 028102 (2011).

[26] J. K. Parrish and W. M. Hamner, *Three Dimensional Animals Groups* (Cambridge University Press, Cambridge, 1997).
[27] B. Szabó, G. J. Szöllösi, B. Gönci, Z. Jurányi, D. Selmeczi, and T. Vicsek, Phys. Rev. E **74**, 061908 (2006).
[28] T. Vicsek, A. Czirók, E. Ben-Jacob, I. Cohen, and O. Shochet, Phys. Rev. Lett. **75**, 1226 (1995).
[29] A. Kudrolli, G. Lumay, D. Volfson, and L. S. Tsimring, Phys. Rev. Lett. **100**, 058001 (2008).
[30] F. Ginelli, F. Peruani, M. Bär, and Hugues Chaté, Phys. Rev. Lett. **104**, 184502 (2010).
[31] G. Gregoire and H. Chate, Phys. Rev. Lett. **92**, 025702 (2004).
[32] Y. K. Tsang, E. Ott, T. M. J. Antonsen, and P. N. Guzdar, Phys. Rev. E **71**, 066313 (2005).
[33] R. Benzi, L. Biferale, R. T. Fisher, L. P. Kadanoff, D. Q. Lamb, and F. Toschi, Phys. Rev. Lett. **100**, 234503 (2008).
[34] G. Sezonov, D. Joseleau-Petit, and R. D'Ari, J. Bacteriol. **189**, 8746 (2007).
[35] J. K. Sveen, *An Introduction to MatPIV v.1.6.1* (University of Oslo, Oslo, 2004), http://folk.uio.no/jks/matpiv/.
[36] F. Peruani, Ph.D. thesis, Technische Universität, 2008.
[37] J. Feder, *Fractals* (Plenum, New York, 1988).
[38] R. Benzi, S. Ciliberto, R. Tripiccione, C. Baudet, F. Massaioli, and S. Succi, Phys. Rev. E **48**, R29 (1993).